Building and Environment 127 (2018) 268–276

Contents lists available at ScienceDirect

Building and Environment

journal homepage: www.elsevier.com/locate/buildenv

Automated mobile sensing: Towards high-granularity agile indoor environmental quality monitoring

Ming Jin[a,*], Shichao Liu[b], Stefano Schiavon[b], Costas Spanos[a]

[a] Electrical Engineering and Computer Sciences Department, University of California, Berkeley, CA 94720, USA
[b] Center for the Built Environment, University of California, Berkekey, CA 94720, USA

ARTICLE INFO

Keywords:
Indoor environmental quality
Mobile sensing
Spatio-temporal interpolation
Robotic sensing
Smart building
Energy efficiency

ABSTRACT

Indoor environmental quality (IEQ) is a critical aspect of the built environment to ensure occupant health, comfort, well-being and productivity. Existing IEQ monitoring approaches rely on sensor networks deployed at selected locations to collect environmental measurements, and are limited in scale and adaptability due to infrastructure cost and maintenance requirement. To enable high-granularity IEQ monitoring with agile adaptation to the dynamic indoor environment, we propose an "automated mobile sensing" system that dispatches a sensor-rich navigation-capable robot to actively survey the indoor space. Data collected in this fashion is sparse in the joint temporal and spatial domain, and cannot be used directly for IEQ evaluation. To deal with this special characteristics, we developed a spatio-temporal interpolation algorithm to capture the global trend and local variation in order to use the data efficiently to reconstruct the IEQ dynamics. We compared the performance of the automated mobile sensing with a dense sensor network in a laboratory where we measured the air-change effectiveness (ASHRAE standard 129) for four different conditions. Results indicate that automated mobile sensing is able to accurately estimate the parameters with a minimal sensor cost and calibration effort. Potential applications of this system include indoor thermal comfort, lighting, indoor air quality and acoustic monitoring, pollutant source identification, and building commissioning. We shared publicly the source codes for robot control, sensor setup, and interpolation algorithm to encourage comparison study and further development.

1. Introduction

Smart buildings are cyber-physical energy systems (CPES) that integrate sensing, data analytics, and control to provide essential services to the occupants. Buildings consume about 40% of primary energy in the U.S. and there is a fundamental drive for buildings to be *energy efficient* [1,2]. As people spend about 90% of their time indoors, they should also be *human-centric* by focusing on improving human health, comfort, well-being and productivity, and well-being [3–6]. This could be achieved effectively by monitoring and enhancing indoor environmental quality (IEQ), such as indoor air quality, thermal comfort, lighting and acoustics [7–9]. IEQ monitoring has been recognized as one of the fundamental strategies to obtain credits by various guidelines and rating systems, such as American Society of Heating, Refrigerating and Air-Conditioning Engineers (ASHRAE)/Chartered Institution of Building Services Engineers (CIBSE)/U.S. Green Building Council (USGBC) Performance Measurement Protocols for commercial buildings (PMP) [10] and Leadership in Energy and Environmental Design (LEED) [11]. For instance, environmental parameters (e.g., temperature, humidity) need to be continuously monitored when occupants take a "right-now" thermal comfort survey, according to AHSRAE/CIBSE/USGBC PMP [10]. LEED suggests CO_2 monitoring in all densely occupied spaces. In addition, IEQ assessment involves contaminants sampling in all occupied spaces, such as volatile organic compound (VOC) and particulate matter (PM) [11]. Guidelines, standards and rating systems recognize that more IEQ monitoring would be valuable but affordability constrain limits what is suggested to be used.

Due to complex indoor structures and dynamic environment, IEQ parameter distributions are often *inhomogeneous*, resulting in spatial variations in thermal environment and indoor contaminant exposure [12–14]. Furthermore, applications of personalized heating/cooling devices, aiming to reduce building energy use, augment such inhomogeneity [15–20]. Consequently, spatio-temporal monitoring of indoor environment can provide an comprehensive IEQ assessment.

Key challenges in the objective IEQ assessment of commercial buildings involve accurate, easy-to-use, and scalable sensing systems [21]. An effective approach is to implement wireless sensor networks; however, despite the continuous reduction in sensor cost and

* Corresponding author.
E-mail addresses: jinming@berkeley.edu (M. Jin), scliu@berkeley.edu (S. Liu), schiavon@berkeley.edu (S. Schiavon), spanos@berkeley.edu (C. Spanos).

https://doi.org/10.1016/j.buildenv.2017.11.003
Received 31 August 2017; Received in revised form 29 October 2017; Accepted 2 November 2017
Available online 06 November 2017

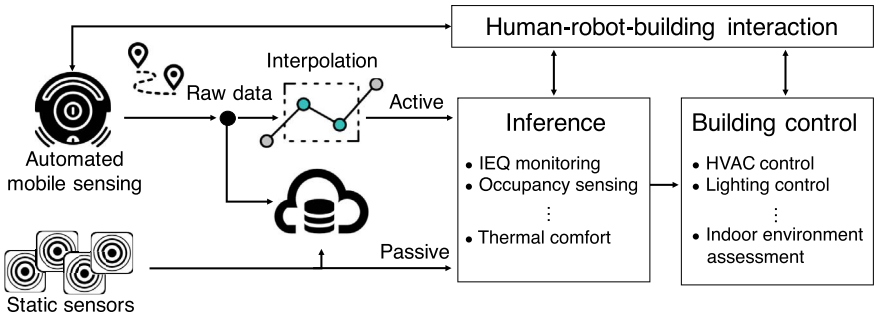

Fig. 1. Automated mobile sensing system overview. The robotic platform can either work alone or with static sensor network to actively estimate building context and facilitate building control.

simplification in deployment, infrastructure investment and maintenance might still remain a concern in the near future, especially when considering monitoring numerous IEQ variables simultaneously. Moreover, many sensors that require a significant amount of power (e.g., hot wire anemometer) can not easily become wireless. Additionally, buildings might undergo several renovations in their lifecycle, so *agility* is essential to adapt to the changing environment.

1.1. Main contributions and objectives

Differentiated from existing approaches of deploying static sensors for indoor monitoring, we propose a sensing paradigm of "automated mobile sensing" by leveraging a navigation-enabled sensing-capable mobile robot (see Fig. 1 for the overall architecture). This represents a paradigm of "active inference", where the robot can plan its path to take representative measurement samples at locations of interests, as compared to "passive inference" where the data collection is limited by the geolocations of static sensors.

From a data analytic perspective, unlike data from static sensors, the samples taken by the robot is highly sparse in time and space, as illustrated in Fig. 3. While existing interpolation mainly focuses on the spatial domain [22,23], we propose a data-efficient spatio-temporal (ST) interpolation method that extracts local and global trends and constructs an informative visualization of IEQ. Through experimental evaluations of zone air distribution effectiveness (air-change effectiveness, ACE), automated mobile sensing is compared with static sensing with a dense sensor network required by the ASHRAE standard 129 [24]. Note that the air-change effectiveness experiment is only used to demonstrate our novel platform, rather than to investigate possible factors that influence its value, for which we refer the readers to more established works [20,25–27]. It is, therefore, the objective of this paper to describe the novel "automated mobile sensing" system for indoor environmental quality monitoring, enabled by a sensor-rich navigation-capable robot to actively survey the indoor space.

2. Brief literature review

2.1. Indoor environmental quality assessment

IEQ assessment can be conducted using occupant surveys [5,28–30], personal monitoring [31–33], and sensor measurements [34–36]. Surveys provide subjective IEQ evaluation from occupant perspectives; however, survey design requires systematic effort to avoid bias and confusion, and the results can not be updated frequently due to user fatigue. Several online or mobile tools have been developed to allow users to vote their thermal or lighting preferences in real time [17,28]; however, the responses may reveal only subjective perceptions, like "the air is stale", but it rarely gives hints about the causes, such as increased indoor pollution caused by low outdoor air flow rate or unpleasant thermal environment due to malfunctioning mechanical systems.

Objective measurements, taken by static or mobile sensors during daily operation or performance commissioning, can accurately depict building environment and diagnose potential faults. Static sensors are deployed in a space to continuously monitor environmental parameters [1]; nevertheless, limited by cost, the deployment is often sparse in locations or absent, especially for expensive sensors like CO_2. In addition, while indoor environment is often inhomogeneous and unpredictable, the stationary sensors may not always be deployed in the optimal locations to reflect indoor environment. Personal monitoring systems, such as using infrared thermography [31] and physiological measurements [32,33,37] can offer assessment of individual comfort and inform building operation system of proper adjustments in real-time; however, they require users to be equipped with special instruments or sensors and may involve privacy concerns. For some IEQ parameters like indoor air quality, the effect on productivity and health may be long-term and cannot be readily captured by physiological measurements.

Mobile carts, such as an instrumented chair-like cart [34] and the IEQ cart [35,36] can hold multiple sensors to take measurements simultaneously at a given location. While the results are comprehensive, the carts often require considerable labor cost and manual navigation. Several studies exist to deploy robots for monitoring and identifying pollutants both indoor and outdoor [38–41]; however, the methods do not distinguish the global trend of physical parameters from their local variations, which might lower the estimation accuracy, and the results have not been validated against a ground truth, which requires a dense sensor network for comparison.

2.2. Continuous interpolation from discrete measurements

Data from static or mobile sensor measurements is highly sparse and requires interpolation for informative visualization. Spatial interpolation is a well-studied topic in geostatistical analysis and image processing communities, where methods like Kriging and Markov random field (MRF) are among the most prominent [22,23]. Kriging has also been combined with Gaussian MRF [42], Bayesian network [43], and principle component analysis [44] to improve the computational efficiency. In practice, this means that the algorithm can analyze a large amount of data within limited time span, thus enabling large-scale sensing.

Since Kriging is efficient with sparse data, it has been generalized to spatio-temporal interpolation [22,45]. Shape functions have also been introduced based on finite element mesh generation [46]. Variational Gaussian-process factor analysis is proposed to model the dynamics of spatio-temporal data [47]. Prior works assume multiple time series data from individual sensor stations, which requires continuity in time at a specific location; but the data from mobile sensing robot poses the challenge of high sparsity and non-continuity in time and space (Fig. 3).

Differentiated from existing interpolation methods, our method can efficiently capture spatial and temporal dynamics by constructing global and local trend estimators based on highly sparse data.

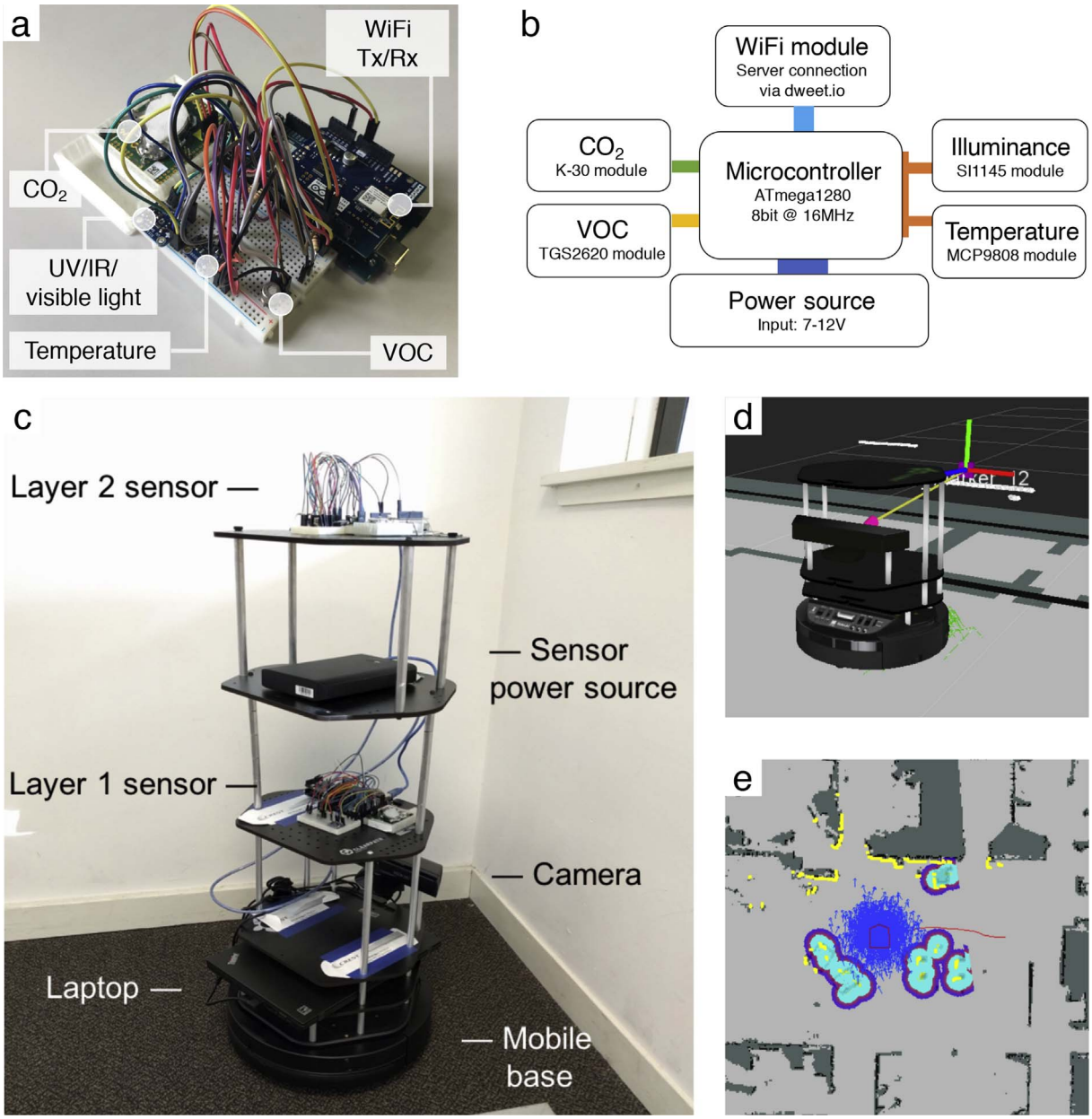

Fig. 2. (a) Snapshot of the environmental sensing platform. (b) Schematic of sensor integration and data communication. Snapshots of (c) the robotic platform, (d) Augmented reality tag indoor positioning, and (e) camera-enabled simultaneous localization and mapping (SLAM).

3. Methodology

3.1. Integrated system architecture

This section introduces the environmental sensing platform and the robotic base (Fig. 2) as the essential components in the autonomous sensing system.

Based on an Arduino microcontroller board, the environmental sensing platform (ESP) is designed on a software-level to detect and report sensor faults automatically to alert users, and to work instantly once powered on, relieving laborious configuration or setup (Fig. 2).

A comprehensive list of sensors are integrated in the ESP to monitor indoor environmental parameters, including temperature and humidity, light level, PM2.5, CO_2, and organic volatile compound (VOC) (Table 1). Data are sampled and uploaded to a server using a WiFi communication link at an interval of 10 s, which are also pushed to a front-end visualization portal (hosted at dweet.io) for real-time monitoring. In addition, all sensors are calibrated using automatic baseline correction (ABC) beforehand. In particular, we calibrated the CO_2 sensors (K-30) using an off-the-shelf HOBO MX1102 CO_2 logger.

Programmed under the robot operating system (ROS), a collection of software frameworks for robot software development, it runs mapping, positioning, and navigation algorithms autonomously. Mounted with ESP, the mobile robot (Turtlebot 2) can be controlled remotely or make decisions based on real-time sensing data (Fig. 2).

3.1.1. Indoor positioning

In a new and dynamic environment, the robot can operate without a detailed floormap. Based on the depth image from Kinect camera, the Simultaneous Localization and Mapping (SLAM) problem is solved with particle filter by tracking the robot position relative to the surroundings [48] (Fig. 2e).

With the additional user-provided layout, a higher-precision location estimation is enabled by an augmented reality tag system (Fig. 2d). Upon the initial positioning by SLAM, the estimate is updated by reading the distance and direction to nearby reference points marked by

Table 1
Sensing modules of ESP.

Environmental parameter	Module	Performance	Price
Temperature	MCP9808	Accuracy: 0.25 °C typical precision over −40 °C to 125 °C range	$4.68
Illuminance	SI1145	Resolution: 100 mlx	$9.95
CO_2	K-30	Measurement range: 0–10000 ppm Accuracy: ± 3% of measurement Response time: 20 s diffusion time	$85
PM2.5	SEN0177	Measuring pm range: 0–500 μg/m^3	$46.90
Organic volatile compound	TGS2620	Typical detection range: 50–5000 ppm Sensitivity: 0.3–0.5 in ethano	$8.90

augmented reality tags, which are fiducial markers deployed in advance at locations indicated on the room layout. During the positioning process, the relative distances and angles are processed by the triangulation algorithms to revise the location estimate [49]. This also enables more robust estimation against dynamic changes in the room as long as the augmented reality tags remain visible to the robot [49].

3.1.2. Navigation and collision avoidance

Given a set of goal points, the robot is navigated using a *global planner* to set the shortest path based on the current knowledge about the space. However, when some moving objects, like occupants, obstruct the planned path, a *local planner* is employed to avoid obstacles. Supported by ROS, robot specs like velocity, angular speed, and goal tolerance can be set to accommodate specific requirements.

3.2. Spatio-temporal interpolation algorithm

Compared to data collected by static sensor stations, measurements from mobile sensors cover the whole space with higher granularity; however, for each location, the samples are conducted sequentially in multiple locations (see Fig. 3 for an illustration). The problem is stated as below:

Given the mobile sensing data $\mathscr{D} = \{(\boldsymbol{s}_1, t_1, v_1), \ldots, (\boldsymbol{s}_n, t_n, v_n)\}$, where $\boldsymbol{s}_i = (x_i, y_i)$ and t_i are the spatial coordinate and timestamp, and v_i is the actual value, our goal is to find a function, $\hat{f}: \mathbb{R}^2 \times \mathbb{R} \mapsto \mathbb{R}$, which estimate values at unexplored locations at certain time.

A data-driven approach to spatio-temporal (ST) interpolation is adopted based on statistical decision theory. The variation of an indoor environment exhibits both a global trend, as dominated by outdoor weather, building envelope and Heating, Ventilation and Air Conditioning (HVAC) operation, as well as a local trend, as influenced by occupants, inhomogeneous air turbulence, pollutant source, and furniture.

The proposed algorithm, therefore, has three key steps (Fig. 4):

1. ST binning: consider a 3D-space (*xy* and *t* axes represent space and time, respectively) divided into 3D cubes based on spatial and temporal resolutions. Data points are binned and aggregated to reduce measurement errors.
2. Global trend extraction: a regression trend is fitted by, e.g., locally weighted scatterplot smoothing (LOWESS) [50], to capture the global variation.
3. Local variation estimation: based on the residues from global trend, a local variation function is approximated and applied on unknown points.

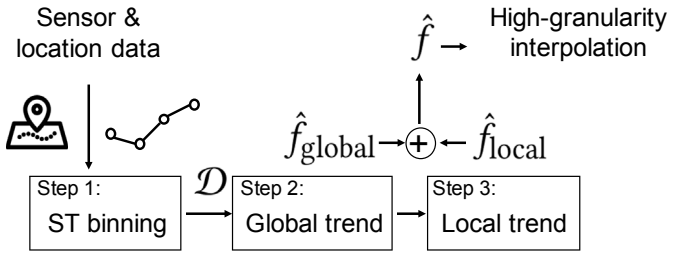

Fig. 4. Illustration of the ST interpolation algorithm, including ST binning for data smoothing, global trend extraction, and local variation estimation. The outcome is an interpolation function $\hat{f}$ that encodes a high-granularity interpolation map.

The high-granularity map that depicts the indoor environment evolution is embedded in the ST interpolation function, given by:

$$\hat{f}(\boldsymbol{s}, t) = \hat{f}_{\text{global}}(t) + \hat{f}_{\text{local}}(\boldsymbol{s}, t), \tag{1}$$

where $\hat{f}_{\text{global}}(t)$ and $\hat{f}_{\text{local}}(\boldsymbol{s}, t)$ are the global and local trends, obtained as follows.

The global trend depicts the average evolution of the phenomenon independent of individual locations, since *data pooling provides sufficient samples for estimation*. Based on the locally weighted scatterplot smoothing (LOWESS) method [50], the global trend, $\hat{f}_{\text{global}}(t)$, at time $t \in [t_c - h(t_c), t_c + h(t_c)]$, is given by:

$$\hat{f}_{\text{global}}(t) = \beta_0 + \beta_1(t - t_0) + \frac{1}{2}\beta_2(t - t_0)^2,\ t \in [t_c - h(t_c), t_c + h(t_c)] \tag{2}$$

where t_c is the center point, $h(t_c)$ is the smoothing span, and $\beta_0, \beta_1, \beta_2$ are parameters given by:

$$(\beta_0, \beta_1, \beta_2) = \operatorname{argmin} \sum_{i=1}^{n} w_i(t_c)\left(v_i - \left(\beta_0 + \beta_1(t_i - t_c) + \frac{1}{2}\beta_2(t_i - t_c)^2\right)\right)^2 \tag{3}$$

where $w_i(t_c) = W\left(\frac{t_i - t_c}{h(t_c)}\right)$ and $W(u) = \begin{cases} ((1 - |u|^3)^3 & |u| \le 1 \\ 0 & |u| > 1 \end{cases}$ obtain the data point weights.

While the global trend function is applicable to all locations, the local function $\hat{f}_{\text{local}}$ captures the spatial variation, which is encoded in the residuals $r_i = v_i - \hat{f}_{\text{global}}(t_i)$. Based on the *empirical risk minimization (ERM)*:

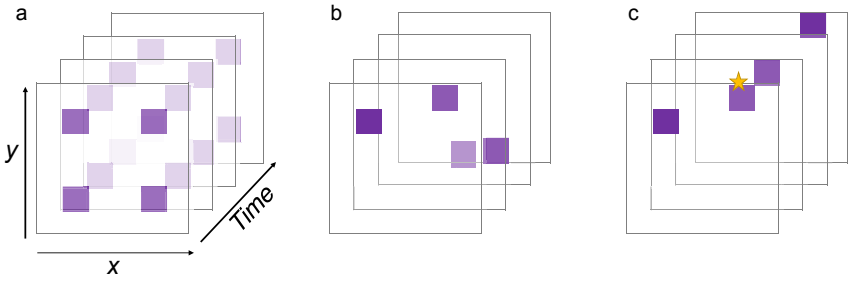

Fig. 3. Illustration of data characteristics in the spatial and temporal domains for (a) static stations, (b,c) automated mobile sensing, where (c) depicts a situation of active exploration around the spot of critical event (star).

$$\hat{f}_{\text{local}} = \underset{f \in \mathcal{F}}{\operatorname{argmin}} \frac{1}{n} \sum_{i=1}^{n} l(f(\boldsymbol{s}_i, t_i), r_i) \tag{4}$$

where $\mathcal{F}$ delineates the range of estimators, e.g., the class of linear regressors, and l: $\mathbb{R} \times \mathbb{R} \rightarrow \mathbb{R}$ is the loss function, which penalizes error in estimation, e.g., the squared loss $l(a, b) = (a - b)^2$. Implicitly, we assume that points close in space and time are also close in values, which is generally true for indoor environment.

A variety of algorithms to capture local variation have been implemented in our open toolset, such as K-nearest neighbor (KNN), Lasso, support vector regression (SVR), adaptive boosting (AdaBoost), random forest, and extra trees [50], which are trained by ERM with different loss functions. The implementation code in Python is available (see the link in section 5.3).

4. Experiments

4.1. Environmental chamber

The experiment took place in a climate chamber in the Center for the Built Environment (CBE), which can precisely control supply airflow rate, indoor temperature (± 0.5 °C) and humidity (± 3%). The ventilation system employs underfloor air distribution (UFAD), where air is supplied from one or two linear grille diffusers on the floor (shown in Fig. 5). By providing cool air at a low momentum from the floor level and utilizing buoyancy generated from indoor heat sources (e.g., occupants) to displace room air, UFAD often achieves a thermally stratified air distribution. During the experiment, all supply air came from outside, and there was not circulated air. We assumed that outdoor air CO_2 concentration was 400 ppm. The supply air flowrate during the experiments was maintained at 79 ± 11 m^3/hr.

As for heat sources, two sedentary thermal manikins, each with total sensible heat loss of 68.7 W (± 5%) were placed, representing female subjects for office work (Fig. 5). In addition, we placed one heater panel (size: 0.5 × 0.2 m; power: 200 W) under each table to investigate how personal heating device affected the zone air distribution effectiveness and examined the robustness of the algorithms in the given experimental setup.

Ten (10) ESPs were deployed in the occupied zone, which measured CO_2 concentrations at 10 locations and provided the standard assessment of air-change effectiveness according to the ASHRAE standard 129. The sensors were placed at a height of 1.5 m, where detailed locations are shown in Fig. 5.

4.2. Description of air-change effectiveness

According to the ASHRAE standard 129 [24] the air-change effectiveness (ACE) is "*a measure of the effectiveness of outdoor air distribution to the breathing level within the ventilated space*". It is also known as "*zone air distribution effectiveness*" [51]. ACE is calculated from the age of air. The age of air is the "*average time elapsed since molecules of air in a given volume of air entered the building from outside*", in other words, the age of air at a specific location in a building refers to the time for a bulk of outdoor air to reach the position after entering the building. A "younger" age of air represents that the air is fresher, which is often located around supply diffusers. An indoor space with a smaller age of air on average often has a higher ventilation efficiency and air quality.

According to ASHRAE standard 129, the age of air can be estimated using a tracer gas step-up or decay procedure (described in Section 4.3), which often uses non-toxic, non-flammable, and environmentally friendly gases like CO_2 as the tracer gas [24]. The ISO 16000 standard also describes the use of a single tracer gas to determine the local mean age of air by using concentration decay or homogeneous constant emission [52]. According to the decay procedure, the air age $A(\boldsymbol{s})$ at location $\boldsymbol{s}$ is given by:

$$A(\boldsymbol{s}) = (t_{stop} - t_{start}) \frac{C_{avg}(\boldsymbol{s})}{C(\boldsymbol{s}, t_{start})}, \tag{5}$$

where t_{start} is the time at the beginning of the decay, t_{stop} is the time when the procedure ends, $C(\boldsymbol{s}, t)$ is the tracer gas concentration at location $\boldsymbol{s}$ at time t, and $C_{avg}(\boldsymbol{s})$ is the time-averaged concentration between t_{start} and t_{stop}. Since the samples are usually discrete in time, the time-averaged concentration $C_{avg}(\boldsymbol{s})$ can be estimated by $\frac{1}{n}\sum_{i=1}^{n} C(\boldsymbol{s}, t_{start} + i\Delta_t)$, where Δ_t is the sampling interval, and n is the number of samples between t_{start} and t_{stop}.

Based on the air age measurement, the ACE $E(\boldsymbol{s})$ is given by Ref. [24]:

$$E(\boldsymbol{s}) = \frac{A(\boldsymbol{s}_{ex})}{A(\boldsymbol{s})}, \tag{6}$$

where $A(\boldsymbol{s}_{ex})$ indicates the age of air at the exhaust vent. By definition, this metric describes an air distribution system's capacity to deliver ventilated air to an indoor space. The local ACE represents the effectiveness of outdoor air delivery to one specific point in a space.

The ACE is typically 1.0 for a well mixing ventilation system in cooling and equal or higher than 1.2 for displacement ventilation [51]. In general, a space with a higher ACE is associated with a better air distribution system.

4.3. Experimental procedure

The experimental procedure was designed according to the standard tracer-gas decay process by ASHRAE standard 129, as follows:

1. First, beverage-grade CO_2 was injected into the chamber with a ceiling fan and a standing fan well mixing the injected CO_2

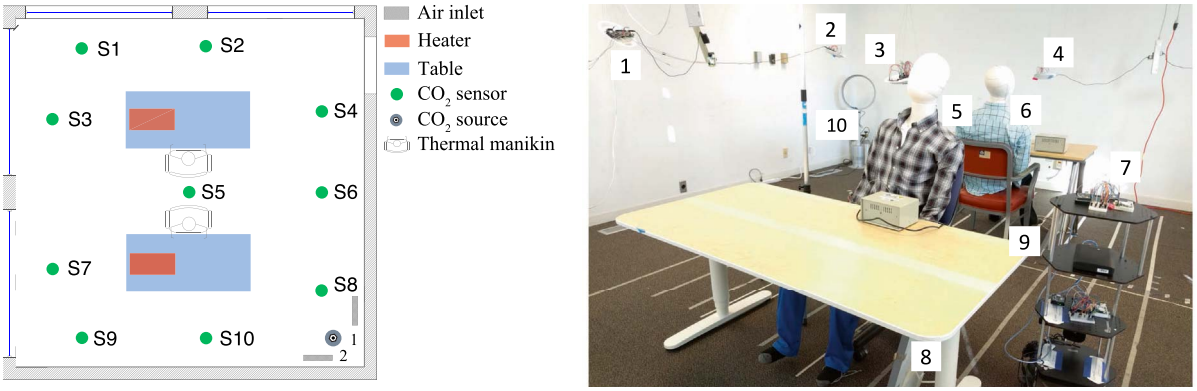

Fig. 5. Left: testbed floorplan, showing the air inlet diffusers, heaters, tables, CO_2 sensor and source locations, and thermal manikins. The sensors are placed at a uniform height of 1.5 m. Right: testbed snapshot, showing the static sensor stations (1–4), thermal manikins to model realistic heat sources (5,6), robot (7), floor heaters (8,9), and CO_2 source (10).

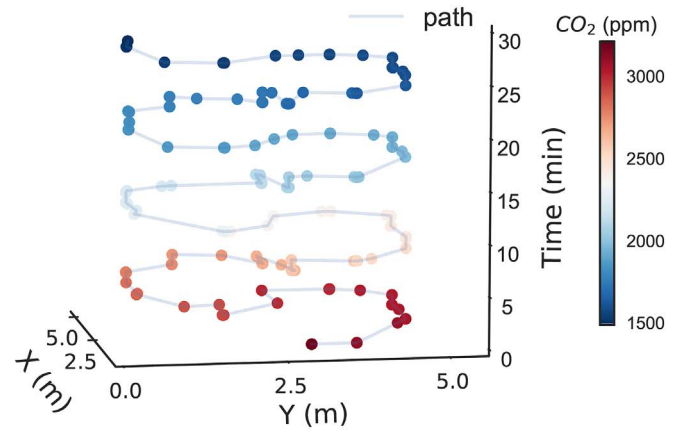

(a) Spatio-temporal view.

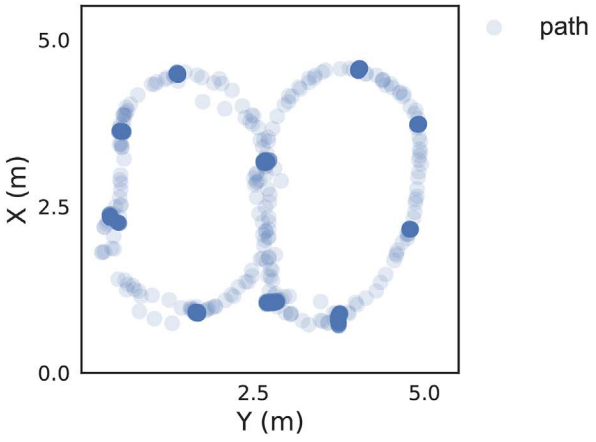

(b) Plane view.

Fig. 6. (a) Spatio-temporal trace of mobile measurements. (b) Plane view of the visiting trace of the robot.

Table 2
Experimental conditions for vents and heater status.

Experiment i.d.	Exp A	Exp B, C	Exp D	Exp E
Supply diffusers	Diffuser 1	Diffuser 1 & 2	Diffuser 1	Diffuser 1 & 2
Floor heater status	Off	Off	On	On

throughout the chamber. It was assumed that CO_2 was well mixed in the chamber short after the injection period [53].

2. When indoor CO_2 concentration was elevated to approximately 3000 ppm, we turned off the CO_2 injection and ceiling fans. The injection period took roughly 5 min.
3. After the ceiling fans were off, the indoor airflow pattern was re-established after 5 min [54].
4. The automobile platform measured CO_2 concentration from the start location and moved to the next one. Fig. 6 illustrates the moving route of the platform that stayed at each location for 45 s for CO_2 sampling. The platform moved at a speed of 2 m/s to the next location until the completion of CO_2 recording at all locations. The moving speed was optimized so that airflow pattern was disturbed at a minimum level and CO_2 decay at 10 locations can be captured in roughly 8 min.

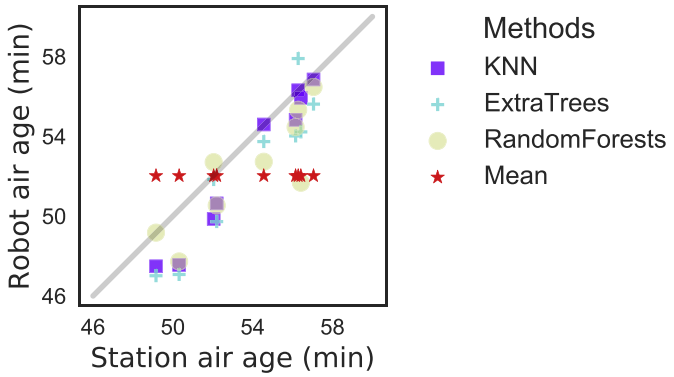

Fig. 8. Plot of air age estimation by static stations and mobile robot with different local variation methods in Exp B.

We compared ACE at various air distribution conditions measured by the mobile sensing with that obtained according to ASHRAE standard 129 to validate the performance of the automobile platform. Table 2 describes the investigated scenarios by altering the intensities of supply air momentum and heat sources, which influences zone air distribution effectiveness as represented by ACE. It is worth noting that the main goal for varying indoor configurations was to validate the reliability of the platform rather than thoroughly examining how ACE could be influenced accordingly. In addition, we repeated one scenario twice (Exp B &C) to assess the repeatability of the indoor air evaluation and the robustness of mobile sensing. Supply airflow rate remained constant for all the scenarios.

5. Results and discussion

We conducted the experiments listed in Table 2 with the robot, where the stationary sensors were used as the standard results for comparison. For each experiment, the robot collected a dataset, $\mathscr{D}$, which was used to train both the global and local trend estimators in (1).

5.1. Age of air

Firstly, we demonstrate that the mobile sensing captures the actual dynamics of CO_2 concentration in the space. Since the measurements from the mobile robot change in both space and time, we visualize CO_2 concentrations of mobile sensors and compare them with the stationary data, shown in Fig. 7. While the mobile data reveals the overall decay trend, it also effectively differentiate the spatial distribution of CO_2 at different locations, which is helpful to build the local trend estimator

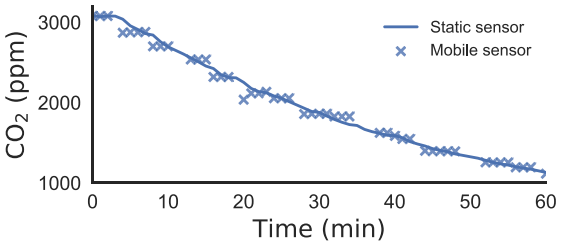

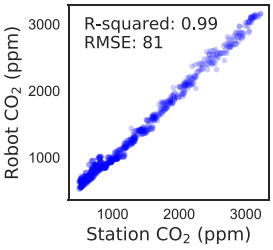

Fig. 7. Left: collocation of the sensor measurements from the static station S5 (lines) and the mobile robot (crosses). Right: comparison of station and robot measurements at the same location and time. This indicates that the robot measurements are representative of the spatial temporal concentrations.

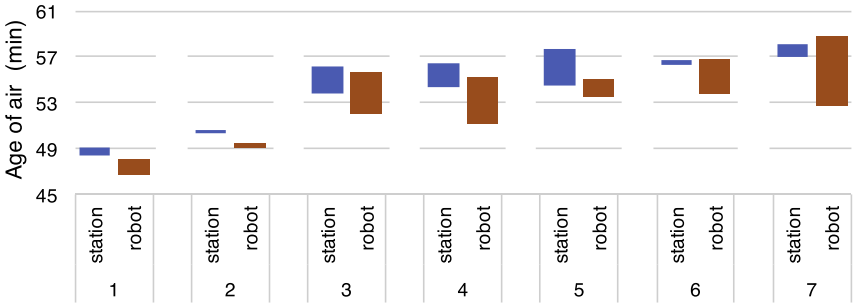

Fig. 9. Comparison of air age estimation given by the stations (blue) and robot (red) at 7 distinct locations in the repeated experiments (Exp B and C). The box indicates the min/max range of estimation across two experiments. (For interpretation of the references to colour in this figure legend, the reader is referred to the web version of this article.)

Table 3
Comparison results of RMSE for ACE estimation and the corresponding Pearson correlation coefficients (reported in brackets) between the static stations and robot estimation. Mean: baseline estimation. Other algorithms represent different local variation estimators.

	Mean	OLS	Ridge	AdaBoost	SVR	KNN	RandForest	ExtraTrees
Exp A	0.077 [0.00]	0.074 [0.73]	0.074 [0.73]	0.058 [0.81]	0.071 [0.82]	0.076 [0.63]	0.072 [0.74]	0.070 [0.76]
Exp B	0.061 [0.00]	0.027 [0.96]	0.027 [0.96]	0.038 [0.77]	0.039 [0.97]	0.031 [0.99]	0.033 [0.91]	0.030 [0.98]
Exp C	0.089 [0.00]	0.078 [0.79]	0.078 [0.79]	0.072 [0.82]	0.066 [0.88]	0.074 [0.82]	0.068 [0.85]	0.071 [0.88]
Exp D	0.043 [0.00]	0.036 [0.62]	0.036 [0.62]	0.031 [0.76]	0.041 [0.84]	0.029 [0.81]	0.031 [0.84]	0.029 [0.81]
Exp E	0.044 [0.00]	0.044 [0.80]	0.044 [0.80]	0.050 [0.79]	0.039 [0.77]	0.045 [0.82]	0.044 [0.73]	0.047 [0.73]

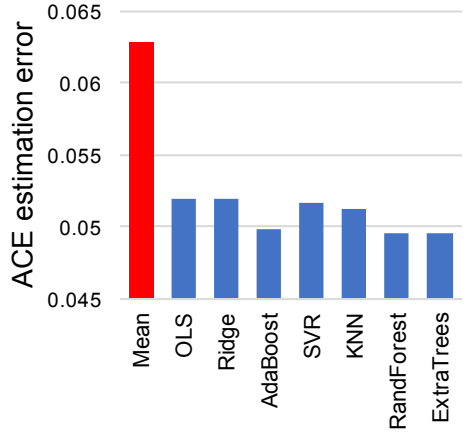

Fig. 10. Average estimation error of ACE for different methods, where Mean is the baseline method. The RMSE of Mean reflects the standard deviation of ACE across the space. The reduced RMSE enables accurate differentiation of ACE at different locations.

(Section 3.2). Indeed, by comparing the robot measurements with the station data collected at the same time and location, we can see that they are almost identical (right plot of Fig. 7).

To evaluate the accuracy of different interpolation algorithms outlined in Section 3.2, we compare the age of air (see Equ. 5) estimated by the robot to the estimation by static sensors, as is shown in Fig. 8. The baseline method, denoted as "Mean", conducts the *global trend estimation* (Equ. (2)) *but disregards the local variation* (Equ. (4)), thus creating a uniform estimation across the space. On the contrary, methods based on KNN, random forests, and extra trees distinguish the spatial distributions and produce estimation very close to the static measurements (Fig. 7). Furthermore, for the same ventilation setups, the robot estimation exhibits little variation in the repeated experiments (Exp B and C), comparable to the station performance (Fig. 9), implying that the influence of robot movement on CO_2 distribution is negligible.

5.2. Air-change effectiveness

As for the ACE evaluation, results indicate that the proposed

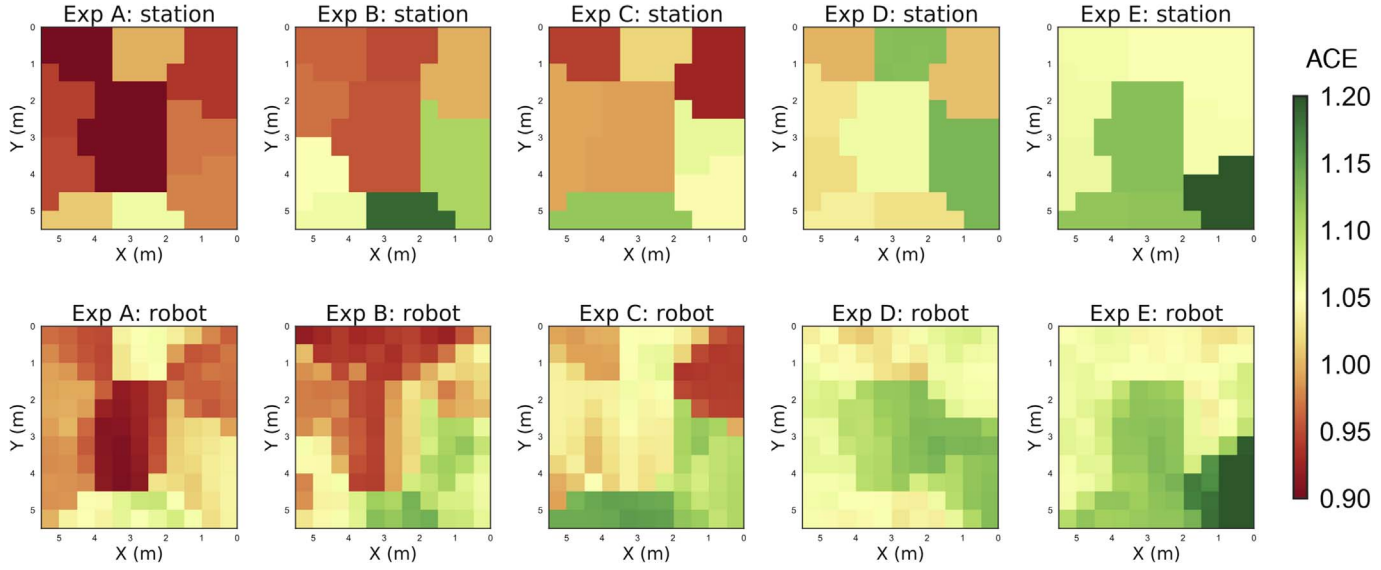

Fig. 11. Visualization of spatial distribution of ACE parameters estimated by the static sensors (top plots) and the robotic platform (bottom plots). The five experimental conditions are listed in Table 2.

interpolation methods significantly outperform the baseline model (Table 3 lists the mean squared error for all the experiments, and Fig. 10 illustrates the average performance). Since the typical values of ACE are around 1, the reduction of RMSE from 0.063 (Mean) to 0.049 (ExtraTrees) in Fig. 10 is significant from a practical point of view, which also enables more accurate depiction of the spatial differences of ACE. The Pearson correlation coefficients are close to one for the list of algorithms, indicating that the ACE estimation from interpolated robotic measurements follow the same trend as the station estimation. However, some algorithms like Ridge had relatively low correlation coefficient of 0.62 for Exp D, which was outperformed by Random Forest with coefficient of 0.84. This indicates that Random Forest had a better generalization capability than Ridge for interpolation at unknown points. In addition, it can be observed that the correlation coefficients of Random Forest are relatively low for Exp A and E as compared to the others, since the spatial variation of ACE in these two experiments was not substantial as indicated by the static sensor measurements in Fig. 11. Note that the correlation for Mean method is 0 because the prediction from Mean is a constant, which fails to capture the spatial variation of ACE across the chamber.

The ACE measurements shows the ventilation effectiveness of the different system configurations. In Fig. 11, ACE results for the static and the robot case are shown. For the robot data the interpolation is done using KNN to produce a high-granularity ACE mapping. The visualization indicates that ACE improves with reducing mixing effects with more supply vents (Exp B, C, E) and adding heating sources (Exp D and E)for the given indoor configuration in this study. The results are expected. The air distribution system with two supply diffusers reduces supply air momentum and mixing effects, resulting in a higher thermal stratification in the room. In addition, the heaters under the tables also increase thermal stratification, while minimizing the potential disruption in terms of thermal plumes to room airflow. The increased thermal stratification helps generate displacement ventilation in the room and improve ACE.

5.3. Potential applications

The proposed method is able to capture indoor environmental parameters both spatially and temporally. The approach can significantly reduce the sensing infrastructure cost.[1] It could be applied to assess indoor environmental quality and for continuous commissioning. In the future deployment, the robot can rover around a space to continuously monitor indoor IEQ, and can meanwhile interact with users and facilitate automatic building control, which allows for active inference and decision making in real-time building operation. Since the robot can move at a speed of about 2 m/s, one single robot is needed to cover a typical office building floor, though it cannot yet climb the stairs or navigate between floors.

It has capacities to navigate across large indoor spaces to search locations where local environment is unacceptable. Pollutant sources (e.g., particles from occupants or penetrated through open windows) may be hard to capture using a limited number of stationary sensors. This platform can access an indoor space extensively and it could be modified to *identify pollutant sources* through active sampling (see Fig. 3c).

Building system commissioning could also employ the platform to diagnose the efficacy of HVAC and lighting systems. For instance, non-uniformity of air temperature in the underfloor air distribution (UFAD) plenum indicates an ineffective system design or implementation. The platform can map the temperature distribution inside the plenum which is often not easily accessible for traditional temperature monitoring (e.g., thermistor probe deployment). Moreover, low ventilation effectiveness in terms of supply air short-circuit is not uncommon for HVAC operated at heating mode [55]. The proposed system could assess indoor ACE without deploying dozens of trace gas sensors [24]. Nevertheless, the platform may not be suitable in residential houses where compact furniture and stairs may limit the moving range of the platform. The source codes for robot control, sensor setup, and ST algorithm are made available at http://www.jinming.tech/software/ to encourage comparison study and further development in this area.

[1] The robot employed in the study is TurtleBot 2, which costs about 2000 USD: http://www.turtlebot.com/turtlebot2/ [access date: 10/2017].

6. Conclusion

This study proposed the “automated mobile sensing” paradigm for high-granularity, agile and scalable indoor environmental quality monitoring. The integrated sensing system consists of a mobile base and an environmental sensing platform which is capable of measuring a range of environmental parameters. To derive actionable insights from the collected data that are sparse in both spatial and temporal domains, we developed a spatio-temporal interpolation algorithm that leverages a hierarchical approach to reconstruct continuous mapping of the indoor environment. We demonstrated the mobile platform in a laboratory experiment of measuring air-change effectiveness. By comparing the measurements from the mobile platform and those from a standard dense sensor network, we showed that the automated mobile sensing approach was able to determine the air-change effectiveness with high spatial granularity and accuracy.

Acknowledgements

This research is funded by the Republic of Singapore's National Research Foundation through a grant to the Berkeley Education Alliance for Research in Singapore (BEARS) for the Singapore-Berkeley Building Efficiency and Sustainability in the Tropics (SinBerBEST) Program. BEARS has been established by the University of California, Berkeley as a center for intellectual excellence in research and education in Singapore. We would like to express our gratitude to Fred Bauman for his suggestions during the lab experiments.

References

[1] K. Weekly, M. Jin, H. Zou, C. Hsu, A. Bayen, C. Spanos, Building-in-briefcase (bib), arXiv preprint arXiv:1409.1660.
[2] M. Jin, N. Bekiaris-Liberis, K. Weekly, C.J. Spanos, A.M. Bayen, Occupancy detection via environmental sensing, IEEE Trans. Automation Sci. Eng. 99 (2017) 1–13.
[3] M. Jin, H. Zou, K. Weekly, R. Jia, A.M. Bayen, C.J. Spanos, Environmental sensing by wearable device for indoor activity and location estimation, 40th Annual Conference of the IEEE Industrial Electronics Society, 2014, pp. 5369–5375.
[4] Indoor climate and productivity in offices, REHVA guidebooks 6, in: P. Wargocki, O.A. Seppnen (Eds.), REHVA, Federation of European Heating and Air-conditioning Associations, Brussels, Belgium, vol. 6, 2006.
[5] M. Frontczak, S. Schiavon, J. Goins, E. Arens, H. Zhang, P. Wargocki, Quantitative relationships between occupant satisfaction and satisfaction aspects of indoor environmental quality and building design, Indoor air 22 (2) (2012) 119–131.
[6] M. Jin, R. Jia, C. Spanos, Virtual occupancy sensing: using smart meters to indicate your presence, IEEE Trans. Mob. Comput. 16 (11) (2017) 3264–3277.
[7] J. Sundell, On the history of indoor air quality and health, Indoor air 14 (s7) (2004) 51–58.
[8] K. Parsons, Human Thermal Environments: the Effects of Hot, Moderate, and Cold Environments on Human Health, Comfort, and Performance, CRC press, 2014.
[9] S. Prasow, Acoustics in green buildings: refining the concept of environmentally quality while improving occupant health and productivity synergistically, J. Acoust. Soc. Am. 123 (5) (2008) 3095–3095.
[10] ASHRAE/CIBSE/USGBC, Performance Measurement Protocols for Commercial Buildings, ASHRAE Transactions, American Society of Heating, Refrigerating and Air-Conditioning Engineers, January 1, 2010 ISBN-13: 978-1933742793, ISBN-10: 1933742798, 298 pages.
[11] US Green Building Council, Leadership in Energy and Environmental Design LEED, Building Design and Construction, V4.
[12] W. Zhang, K. Hiyama, S. Kato, Y. Ishida, Building energy simulation considering spatial temperature distribution for nonuniform indoor environment, Build. Environ. 63 (2013) 89–96.
[13] A. Bulińska, Z. Popiołek, Z. Buliński, Experimentally validated cfd analysis on sampling region determination of average indoor carbon dioxide concentration in occupied space, Build. Environ. 72 (2014) 319–331.
[14] M. Jin, N. Bekiaris-Liberis, K. Weekly, C. Spanos, A.M. Bayen, Sensing by proxy:

occupancy detection based on indoor co2 concentration, in: proceedings of the international conference on mobile ubiquitous computing, Syst. Serv. Technol. (2015) 1–10.
[15] A.K. Melikov, Personalized ventilation, Indoor Air 14 (s7) (2004) 157–167.
[16] S. Schiavon, B. Yang, Y. Donner, V.-C. Chang, W.W. Nazaroff, Thermal comfort, perceived air quality, and cognitive performance when personally controlled air movement is used by tropically acclimatized persons, Indoor air 27 (3) (2017) 690–702.
[17] L.J. Ratliff, M. Jin, I.C. Konstantakopoulos, C. Spanos, S.S. Sastry, Social game for building energy efficiency: incentive design, IEEE Annual Allerton Conference on Communication, Control, and Computing, 2014, pp. 1011–1018.
[18] S. Liu, L. Yin, W.K. Ho, K.V. Ling, S. Schiavon, A tracking cooling fan using geofence and camera-based indoor localization, Build. Environ. 114 (2017) 36–44.
[19] H. Zhang, E. Arens, Y. Zhai, A review of the corrective power of personal comfort systems in non-neutral ambient environments, Build. Environ. 91 (2015) 15–41.
[20] D. Faulkner, W.J. Fisk, D.P. Sullivan, D.P. Wyon, Ventilation efficiencies of desk-mounted task/ambient conditioning systems, Indoor Air 9 (4) (1999) 273–281.
[21] D. Heinzerling, S. Schiavon, T. Webster, E. Arens, Indoor environmental quality assessment models: a literature review and a proposed weighting and classification scheme, Build. Environ. 70 (2013) 210–222.
[22] N. Cressie, C.K. Wikle, Statistics for Spatio-temporal Data, John Wiley & Sons, 2015.
[23] S. Geman, D. Geman, Stochastic relaxation, gibbs distributions, and the bayesian restoration of images, IEEE Trans. pattern analysis Mach. Intell. 6 (1984) 721–741.
[24] ASHRAE Standard 129, Measuring Air-change Effectiveness, ASHRAE, Atlanta, GA, US, 1997, pp. 1–20.
[25] W.J. Fisk, D. Faulkner, D. Sullivan, F. Bauman, Air change effectiveness and pollutant removal efficiency during adverse mixing conditions, Indoor Air 7 (1) (1997) 55–63.
[26] M. Krajčík, A. Simone, B.W. Olesen, Air distribution and ventilation effectiveness in an occupied room heated by warm air, Energy Build. 55 (2012) 94–101.
[27] S. Schiavon, F.S. Bauman, B. Tully, J. Rimmer, Chilled ceiling and displacement ventilation system: laboratory study with high cooling load, Sci. Tech. Build Environ. 21 (7) (2015) 944–956.
[28] L. Zagreus, C. Huizenga, E. Arens, D. Lehrer, Listening to the occupants: a web-based indoor environmental quality survey, Indoor Air 14 (s8) (2004) 65–74.
[29] E. Gossauer, A. Wagner, Post-occupancy evaluation and thermal comfort: state of the art and new approaches, Adv. Build. energy Res. 1 (1) (2007) 151–175.
[30] A. Leaman, F. Stevenson, B. Bordass, Building evaluation: practice and principles, Build. Res. Inf. 38 (5) (2010) 564–577.
[31] A. Ghahramani, G. Castro, B. Becerik-Gerber, X. Yu, Infrared thermography of human face for monitoring thermoregulation performance and estimating personal thermal comfort, Build. Environ. 109 (2016) 1–11.
[32] C. Dai, H. Zhang, E. Arens, Z. Lian, Machine learning approaches to predict thermal demands using skin temperatures: steady-state conditions, Build. Environ. 114 (2017) 1–10.
[33] S. Lee, I. Bilionis, P. Karava, A. Tzempelikos, A bayesian approach for probabilistic classification and inference of occupant thermal preferences in office buildings, Build. Environ. 118 (2017) 323–343.
[34] C. Benton, F. Bauman, M. Fountain, A field measurement system for the study of thermal comfort, ASHRAE Trans. 96 (1990) 623–633.
[35] C.-M. Chiang, P.-C. Chou, C.-M. Lai, Y.-Y. Li, A methodology to assess the indoor environment in care centers for senior citizens, Build. Environ. 36 (4) (2001) 561–568.
[36] H. Kim, et al., Field-test of the new ashrae/cibse/usgbc performance measurement protocols for commercial buildings: basic level, ASHRAE Trans. 118 (2012) 135.
[37] S. Takada, S. Matsumoto, T. Matsushita, Prediction of whole-body thermal sensation in the non-steady state based on skin temperature, Build. Environ. 68 (2013) 123–133.
[38] Y. Chen, H. Cai, Z. Chen, Q. Feng, Using multi-robot active olfaction method to locate time-varying contaminant source in indoor environment, Build. Environ. 118 (2017) 101–112.
[39] A. Lilienthal, T. Duckett, Building gas concentration gridmaps with a mobile robot, Robotics Aut. Syst. 48 (1) (2004) 3–16.
[40] M. Reggente, A. Mondini, G. Ferri, B. Mazzolai, A. Manzi, M. Gabelletti, P. Dario, A.J. Lilienthal, The dustbot system: using mobile robots to monitor pollution in pedestrian area, 3rd Biannual International Conference on Environmental Odour Monitoring and Control, vol. 23, 2010, pp. 273–278.
[41] S. Thrun, C. Martin, Y. Liu, D. Hahnel, R. Emery-Montemerlo, D. Chakrabarti, W. Burgard, A real-time expectation-maximization algorithm for acquiring multi-planar maps of indoor environments with mobile robots, IEEE Trans. Robotics Automation 20 (3) (2004) 433–443.
[42] L. Hartman, O. Hössjer, Fast kriging of large data sets with gaussian markov random fields, Comput. Statistics Data Analysis 52 (5) (2008) 2331–2349.
[43] J. Dearmon, T.E. Smith, Gaussian process regression and bayesian model averaging: an alternative approach to modeling spatial phenomena, Geogr. Anal. 48 (1) (2016) 82–111.
[44] D. Mendez, M. Labrador, K. Ramachandran, Data interpolation for participatory sensing systems, Pervasive Mob. Comput. 9 (1) (2013) 132–148.
[45] K.V. Mardia, C. Goodall, E.J. Redfern, F.J. Alonso, The kriged kalman filter, Test 7 (2) (1998) 217–282.
[46] L. Li, P. Revesz, Interpolation methods for spatio-temporal geographic data, Comput. Environ. Urban Syst. 28 (3) (2004) 201–227.
[47] J. Luttinen, A. Ilin, Variational gaussian-process factor analysis for modeling spatio-temporal data, Advances in Neural Information Processing Systems, 2009, pp. 1177–1185.
[48] D. Fox, W. Burgard, F. Dellaert, S. Thrun, Monte carlo localization: efficient position estimation for mobile robots, AAAI 2 (1999) 343–349.
[49] H. Liu, H. Darabi, P. Banerjee, J. Liu, Survey of wireless indoor positioning techniques and systems, IEEE Trans. Syst. Man, Cybern. Part C Appl. Rev. 37 (6) (2007) 1067–1080.
[50] J. Friedman, T. Hastie, R. Tibshirani, The Elements of Statistical Learning vol. 1, Springer series in statistics Springer, Berlin, 2001.
[51] ANSI/ASHRAE, ANSI/ASHRAE 62.1, Ventilation for Acceptable Indoor Air Quality, ASHRAE, Atlanta, GA, US, 2013.
[52] Indoor air technical committee, Part 8: Determination of Local Mean Ages of Air in Buildings for Characterizing Ventilation Conditions, Geneva: International Organization for Standardization (ISO) 16000.
[53] A. Gadgil, C. Lobscheid, M. Abadie, E. Finlayson, Indoor pollutant mixing time in an isothermal closed room: an investigation using cfd, Atmos. Environ. 37 (39) (2003) 5577–5586.
[54] L. Peeters, A. Novoselac, Impact of Human Activity on Unsteadiness of Airflow and Convective Heat Transfer in Indoor Environmental Studies vol. 1, (2011), pp. 495–500.
[55] S. Liu, A. Novoselac, Air diffusion performance index (adpi) of diffusers for heating mode, Build. Environ. 87 (2015) 215–223.